Journal of Solid Mechanics Vol. 13, No. 4 (2021) pp. 427-447
DOI: 10.22034/jsm.2021.1904644.1621

Deformation Field Produced by a Doublet Source in a Half-Space Model

N. Verma*, K. Singh

Department of Mathematics, Guru Jambheshwar University of Science and Technology, Hisar-125001, India

Received 21 July 2021; accepted 24 September 2021

ABSTRACT

Using Galerkin vector approach closed-form analytic expressions for the displacements and stresses caused by a doublet source buried in a homogenous, isotropic, perfectly elastic half-space have been obtained. Further, the viscoelastic deformation field has been obtained by applying the correspondence principle of linear viscoelasticity, assuming the medium to be elastic in dilatation and Kelvin, Maxwell, or SLS (Standard linear solid) type viscoelastic in distortion. The effect of Poisson's ratio on the deformation field due to a doublet source is examined in elastic half-space. The effect of relaxation time on displacement and stress fields is studied due to a doublet source in viscoelastic half-space. The variation of the displacements and stresses with the epicentral distance is studied graphically using MATLAB software. Stresses for a doublet with axis parallel to x-axis attain minimum value for Poissonian half-space. Viscoelastic displacements and stresses attain maxima for the Maxwell model and minima for the Kelvin model.

Keywords : Elastic half-space; Viscoelastic; Kelvin; Maxwell; Standard linear solid.

1 INTRODUCTION

MANY researchers [1-6] have studied the problems related to seismic sources in an elastic medium. Closed analytical expressions for the surface displacements, strains, and tilts due to inclined shear and tensile faults in a half - space for both point and finite rectangular sources have been presented by Okada [7]. In viscoelastic half-space, the displacement and stress field produced by Centre of dilatation and by a pressure source was derived by Bonafede et al [8]. The static and quasi-static deformation due to various seismic sources including Centre of dilatation was obtained by Singh and Singh [9]. For measuring small velocity and attenuation changes in solids, Robert et al. [10] have developed the active doublet method. Haruo Horikawa [11] have discussed the effect of the stress change due to the first earthquake on the occurrence of the second earthquake that occurred in the northwestern part of Kagoshima in 1997. Pandolfi et al. [12] determined the seismic wave velocity changes at Mt. Vesuvius a volcano located in the South-West of Italy using doublets, and the Coda Wave Interferometry (CWI) method. Wang et al. [13] were presented a two new numerical code FORTRAN programs PSGRN and PSCMP for

*Corresponding author.
E-mail address: nishu.gju2016@gmail.com (N. Verma)

modeling co- and post-seismic response of the Earth's crust to earthquakes. The three doublets reported by the Central Weather Bureau in Taiwan was studied by Lin et al. [14]. They observed that static stress field obtained by the first shock in the doublet shows that stress increased substantially in the second shock. Lai et al. [15] have studied the coseismic deformation by analyzing relevant seismic data of the 2005 Ilan earthquake doublet to identify its seismogenic structure and further proposing a model to explain the structure which is responsible to the development of the Ilan plain. Kogan et al. [16] have studied the mechanism of post seismic deformation with initial horizontal velocities and post seismic uplift triggered by the 2006-2007 great Kurli doublet. To obtain regional seismic moment tensors in Ahar earthquake doublet, Donnera et al. [17] inverted the surface waveforms of the two main shocks and 11 aftershocks and by grouping into pure strike-slip (including the first main shock) and oblique reverse mechanism (including the second main shock), the doublet earthquake can be analyzed. Nissen et al. [18] have given limitations of rupture forecasting exposed by instantaneously triggered earthquake doublet. Verma and Singh [19] have studied the deformation field of two welded half-spaces caused by centre of rotation source. A comparative study of deformation field due to center of dilatation and center of rotation in a viscoelastic half-space model has been done by Verma and Singh [20].

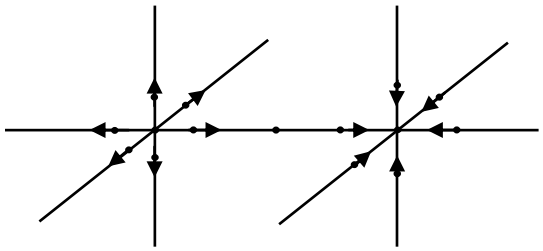

Fig.1
Doublet (double centre of compression-dilatation).

A Doublet is a combination of the double centre of compression – dilatation. These are strikingly similar in terms of magnitude, location, and focal mechanism. By differentiation of center of dilatation, various types of doublets and multiples can be obtained. Application of doublet theory to geomechanics problems has been given by Granik and Ferrari [21] and Ferrari et al. [22]. For these applications, a granular interpretation of doublet mechanics has been employed, in which the material is viewed as an assembly of circular and spherical particles. A pair of such particles represents a doublet as shown in Fig. 2. Corresponding to the doublet (A, B), there exists a doublet connecting the adjacent particle centers and defining the doublet axis. Doublet theory can be used to find a solution to the Flament problem of a concentrated force acting on the free surface of a semi-infinite solid. It has been applied to asphalt concrete materials by Sadd and Dai [23].

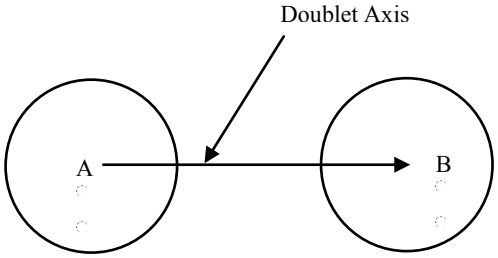

Fig.2
Basic doublet geometry.

In this paper, elastic and viscoelastic deformation of a medium consisting of a homogeneous, isotropic, perfectly elastic half-space due to doublet source, are studied. Numerical results for displacements and stresses are presented graphically. The problem is useful because the interest is about the various phenomena taking place in the earthquakes and measuring of displacements, stresses due to the presence of doublet source. Doublet shocks mechanism may be helpful in reducing the risk for the rescue team.

2 THE GALERKIN VECTOR

Mindlin and Cheng [24] expressed the displacement vector $\vec{u}$ in term of the Galerkin vector $\vec{G}$ through the relation

$$2\,\mu\vec{u} = 2\,(1-\sigma)\nabla^2\,\vec{G} - \nabla\left(\nabla.\vec{G}\right) \tag{1}$$

where μ is the shear modulus and σ is the Poisson ratio. From the Eq. (1), the displacement u_i in the x_i - direction is given by

$$u_i = \frac{1}{2\mu}\left[2\,(1-\sigma)\nabla^2 G_i - \frac{\partial}{\partial x_i}\left(\nabla.\vec{G}\right)\right] \tag{2}$$

where $\vec{G} = G_i\vec{e}_i$ and $\vec{e}_i$ denotes the unit vector in the x_i– direction. The strain-displacement relations are

$$e_{ij} = \frac{1}{2}\left(\frac{\partial u_i}{\partial x_j} + \frac{\partial u_j}{\partial x_i}\right) \tag{3}$$

where e_{ij} is the strain tensor. The stress-displacement relations are

$$\tau_{ij} = \lambda\delta_{ij}u_{n,n} + 2e_{ij}\mu \tag{4}$$

where τ_{ij} is the stress-tensor, δ_{ij} is the Kronecker delta and λ,μ are Lame's constants. From Eq. (1)

$$e_{nn} = \nabla.\vec{u} = \frac{1-2\sigma}{2\mu}\nabla^2\left(div\ \vec{G}\right) \tag{5}$$

The expressions for the Galerkin vectors for a vertical and horizontal concentrated force in a homogeneous, isotropic, elastic half-space were given by Mindlin [25] and Mindlin and Cheng [24]. Let the uniform half-space be $z \geq 0$ with stress free boundary at z=0 and let the point source be located at the point (0,0, c) of the upper half space as shown in Fig. 3. R_1 is the distance between the observer at (*x, y, z*) and the source at (0, 0, c), and R_2 is the distance between the observer at (*x, y, z*) and the image at (0, 0, - c), where

$$R_1^2 = x^2 + y^2 + (z-c)^2 \text{ and } R_2^2 = x^2 + y^2 + (z+c)^2 \tag{6}$$

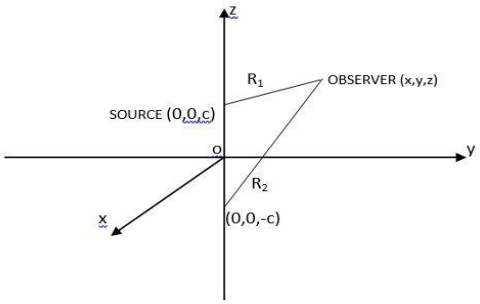

Fig.3
Geometry of a point source in a uniform half-space.

The Strength of doublet parallel to *x*-axis, *y*-axis, and *z*-axis is taken as F_o acts at the point $(0,0,c)$

2.1 Galerkin vector for doublet parallel to the x-axis

$$\vec{G}=\frac{F_o}{8\pi(1-\sigma)}\left[\vec{e}_1\left\{\frac{1}{R_1}+\frac{1-4\sigma}{R_2}\right\}-\vec{e}_3\frac{2xz}{{R_2}^3}\right] \tag{7}$$

2.2 Galerkin vector for doublet parallel to the y-axis

$$\vec{G}=\frac{F_o}{8\pi(1-\sigma)}\left[\vec{e}_2\left\{\frac{1}{R_1}+\frac{1-4\sigma}{R_2}\right\}-\vec{e}_3\frac{2yz}{{R_2}^3}\right] \tag{8}$$

2.3 Galerkin vector for doublet parallel to the z-axis

$$\vec{G}=\frac{F_o\vec{e}_3}{8\pi(1-\sigma)}\left[\frac{1}{R_1}-\frac{1-4\sigma}{R_2}+\frac{2z(z+c)}{{R_2}^3}\right] \tag{9}$$

3 ELASTIC DISPLACEMENT FIELD

3.1 Doublet with an axis parallel to the x-axis

From Eqs. (2) and (7), we obtain the following expressions for the displacement components of Doublet with an axis parallel to the *x*-direction

$${u_1}^{(1)}=\frac{-F_0}{16\pi\mu(1-\sigma)}\left[-\frac{1}{{R_1}^3}-\frac{(3-4\sigma)}{{R_2}^3}+\frac{6z(z+c)}{{R_2}^5}+3x^2\left(\frac{1}{{R_1}^5}+\frac{(3-4\sigma)}{{R_2}^5}-\frac{10z(z+c)}{{R_2}^7}\right)\right] \tag{10}$$

$${u_2}^{(1)}=\frac{-3F_0xy}{16\pi\mu(1-\sigma)}\left(\frac{1}{{R_1}^5}+\frac{(3-4\sigma)}{{R_2}^5}-\frac{10z(z+c)}{{R_2}^7}\right) \tag{11}$$

$${u_3}^{(1)}=\frac{-3F_0x}{16\pi\mu(1-\sigma)}\left(\frac{z-c}{{R_1}^5}-\frac{(3-4\sigma)(z+c)}{{R_2}^5}+\frac{2z}{{R_2}^5}-\frac{10z(z+c)^2}{{R_2}^7}\right) \tag{12}$$

3.2 Doublet with an axis parallel to the y-axis

From Eqs. (2) and (8), we obtain the following expressions for the displacement components of Doublet with an axis parallel to the *y*-direction

$${u_1}^{(2)}=\frac{-3F_0xy}{16\pi\mu(1-\sigma)}\left(\frac{1}{{R_1}^5}+\frac{(3-4\sigma)}{{R_2}^5}-\frac{10z(z+c)}{{R_2}^7}\right) \tag{13}$$

$${u_2}^{(2)}=\frac{-F_0}{16\pi\mu(1-\sigma)}\left[-\frac{1}{{R_1}^3}-\frac{(3-4\sigma)}{{R_2}^3}+\frac{6z(z+c)}{{R_2}^5}+3y^2\left(\frac{1}{{R_1}^5}+\frac{(3-4\sigma)}{{R_2}^5}-\frac{10z(z+c)}{{R_2}^7}\right)\right] \tag{14}$$

$$u_3^{(2)} = \frac{-3F_0 y}{16\pi\mu(1-\sigma)}\left(\frac{z-c}{R_1^5} - \frac{(3-4\sigma)(z+c)}{R_2^5} + \frac{2z}{R_2^5} - \frac{10z(z+c)^2}{R_2^7}\right) \tag{15}$$

3.3 Doublet with an axis parallel to the z-axis

From Eqs. (2) and (9), we obtain the following expressions for the displacement components of Doublet with an axis parallel to the *z*-direction

$$u_1^{(3)} = \frac{-3F_0 x}{16\pi\mu(1-\sigma)}\left(\frac{z-c}{R_1^5} - \frac{(3-4\sigma)(z+c)}{R_2^5} - \frac{2z}{R_2^5} + \frac{10z(z+c)^2}{R_2^7}\right) \tag{16}$$

$$u_2^{(3)} = \frac{-3F_0 y}{16\pi\mu(1-\sigma)}\left(\frac{z-c}{R_1^5} - \frac{(3-4\sigma)(z+c)}{R_2^5} - \frac{2z}{R_2^5} + \frac{10z(z+c)^2}{R_2^7}\right) \tag{17}$$

$$u_3^{(3)} = \frac{-F_0}{16\pi\mu(1-\sigma)}\left[-\frac{1}{R_1^3} - \frac{(3-4\sigma)}{R_2^3} + \frac{3(z-c)^2}{R_1^5} + \frac{3(3-4\sigma)(z+c)^2}{R_2^5} - \frac{18z(z+c)}{R_2^5} + \frac{30z(z+c)^3}{R_2^7}\right] \tag{18}$$

4 ELASTIC STRAIN AND STRESS FIELD

The strain components e_{ij} can be obtained by the strain displacement relations (3) whereas the stresses follow from Eqs. (4) and are obtained below.

4.1 Doublet with an axis parallel to the x-axis

From Eqs. (10)-(12), we obtain the following expressions for the stress components of Doublet with an axis parallel to the *x*-direction

$$\tau_{11}^{(1)} = \frac{-3F_0 x}{8\pi(1-\sigma)}\left[\frac{3}{R_1^5} + \frac{(9-16\sigma)}{R_2^5} - \frac{10(z+c)(3z-2\sigma(z+c))}{R_2^7} - 5x^2\left(\frac{1}{R_1^7} + \frac{(3-4\sigma)}{R_2^7} - \frac{14z(z+c)}{R_2^9}\right)\right] \tag{19}$$

$$\tau_{22}^{(1)} = \frac{-3F_0 x}{8\pi(1-\sigma)}\left[\frac{1}{R_1^5} + \frac{(3-8\sigma)}{R_2^5} - \frac{10(z+c)(z-2\sigma(z+c))}{R_2^7} - 5y^2\left(\frac{1}{R_1^7} + \frac{(3-4\sigma)}{R_2^7} - \frac{14z(z+c)}{R_2^9}\right)\right] \tag{20}$$

$$\tau_{33}^{(1)} = \frac{-3F_0 x}{8\pi(1-\sigma)}\left[\frac{1}{R_1^5} - \frac{1}{R_2^5} - \frac{5(z+c)(5z-c)}{R_2^7} - \frac{5(z-c)^2}{R_1^7} + \frac{10z(z+c)^3}{R_2^9}\right] \tag{21}$$

$$\tau_{12}^{(1)} = \frac{-3F_0 y}{8\pi(1-\sigma)}\left[\frac{1}{R_1^5} + \frac{(3-4\sigma)}{R_2^5} - \frac{10z(z+c)}{R_2^7} - 5x^2\left(\frac{1}{R_1^7} + \frac{(3-4\sigma)}{R_2^7} - \frac{14z(z+c)}{R_2^9}\right)\right] \tag{22}$$

$$\tau_{23}^{(1)} = \frac{-15F_0 x y}{8\pi(1-\sigma)}\left(-\frac{z-c}{R_1^7} - \frac{(3z+c)}{R_2^7} + \frac{14z(z+c)^2}{R_2^9}\right) \tag{23}$$

$$\tau_{31}^{(1)}=\frac{-3F_0}{8\pi(1-\sigma)}\left[\frac{z-c}{R_1^5}+\frac{(3z+c)}{R_2^5}-\frac{10z(z+c)^2}{R_2^7}-5x^2\left(\frac{z-c}{R_1^7}+\frac{(3z+c)}{R_2^7}-\frac{14z(z+c)^2}{R_2^9}\right)\right] \tag{24}$$

4.2 Doublet with an axis parallel to the y-axis

From Eqs. (13)-(15), we obtain the following expressions for the stress components of Doublet with an axis parallel to the *y*-direction

$$\tau_{11}^{(2)}=\frac{-3F_0y}{8\pi(1-\sigma)}\left[\frac{1}{R_1^5}+\frac{(3-8\sigma)}{R_2^5}-\frac{10(z+c)(z-2\sigma(z+c))}{R_2^7}-5x^2\left(\frac{1}{R_1^7}+\frac{(3-4\sigma)}{R_2^7}-\frac{14z(z+c)}{R_2^9}\right)\right] \tag{25}$$

$$\tau_{22}^{(2)}=\frac{-3F_0y}{8\pi(1-\sigma)}\left[\frac{3}{R_1^5}+\frac{(9-16\sigma)}{R_2^5}-\frac{10(z+c)(3z-2\sigma(z+c))}{R_2^7}-5y^2\left(\frac{1}{R_1^7}+\frac{(3-4\sigma)}{R_2^7}-\frac{14z(z+c)}{R_2^9}\right)\right] \tag{26}$$

$$\tau_{33}^{(2)}=\frac{-3F_0y}{8\pi(1-\sigma)}\left[\frac{1}{R_1^5}-\frac{1}{R_2^5}-\frac{5(z-c)^2}{R_1^7}-\frac{5(z+c)(5z-c)}{R_2^7}+\frac{70z(z+c)^3}{R_2^9}\right] \tag{27}$$

$$\tau_{12}^{(2)}=\frac{-3F_0x}{8\pi(1-\sigma)}\left[\frac{1}{R_1^5}+\frac{(3-4\sigma)}{R_2^5}-\frac{10z(z+c)}{R_2^7}-5y^2\left(\frac{1}{R_1^7}+\frac{(3-4\sigma)}{R_2^7}-\frac{14z(z+c)}{R_2^9}\right)\right] \tag{28}$$

$$\tau_{23}^{(2)}=\frac{-3F_0}{8\pi(1-\sigma)}\left[\frac{z-c}{R_1^5}+\frac{(3z+c)}{R_2^5}-\frac{10z(z+c)^2}{R_2^7}-5y^2\left(\frac{z-c}{R_1^7}+\frac{(3z+c)}{R_2^7}-\frac{14z(z+c)^2}{R_2^9}\right)\right] \tag{29}$$

$$\tau_{31}^{(2)}=\frac{-15F_0\,x\,y}{8\pi(1-\sigma)}\left(-\frac{z-c}{R_1^7}-\frac{(3z+c)}{R_2^7}+\frac{14z(z+c)^2}{R_2^9}\right) \tag{30}$$

4.3 Doublet with an axis parallel to the z-axis

From Eqs. (16)-(18), we obtain the following expressions for the stress components of Doublet with an axis parallel to the *z*-direction

$$\tau_{11}^{(3)}=\frac{-3F_0}{8\pi(1-\sigma)}\left[\begin{array}{l}\dfrac{z-c}{R_1^5}-\dfrac{(3-16\sigma)(z+c)}{R_2^5}-\dfrac{2z}{R_2^5}+\dfrac{10(z+c)^2(z-2\sigma(z+c))}{R_2^7}\\ -5x^2\left(\dfrac{z-c}{R_1^7}-\dfrac{(3-4\sigma)(z+c)}{R_2^7}-\dfrac{2z}{R_2^7}+\dfrac{14z(z+c)^2}{R_2^9}\right)\end{array}\right] \tag{31}$$

$$\tau_{22}^{(3)}=\frac{-3F_0}{8\pi(1-\sigma)}\left[\begin{array}{l}\dfrac{z-c}{R_1^5}-\dfrac{(3-16\sigma)(z+c)}{R_2^5}-\dfrac{2z}{R_2^5}+\dfrac{10(z+c)^2(z-2\sigma(z+c))}{R_2^7}\\ -5y^2\left(\dfrac{z-c}{R_1^7}-\dfrac{(3-4\sigma)(z+c)}{R_2^7}-\dfrac{2z}{R_2^7}+\dfrac{14z(z+c)^2}{R_2^9}\right)\end{array}\right] \tag{32}$$

$$\tau_{33}^{(3)} = \frac{-3F_0}{8\pi(1-\sigma)}\left[\frac{3(z-c)}{R_1^5}+\frac{3(z+c)}{R_2^5}-\frac{6z}{R_2^5}-\frac{5(z+c)^3}{R_2^7}-\frac{5(z-c)^3}{R_1^7}+\frac{60z(z+c)^2}{R_2^7}-\frac{70z(z+c)^4}{R_2^9}\right] \tag{33}$$

$$\tau_{12}^{(3)} = \frac{-15F_0 x y}{8\pi(1-\sigma)}\left(-\frac{z-c}{R_1^7}+\frac{(3-4\sigma)(z+c)}{R_2^7}+\frac{2z}{R_2^7}-\frac{14z(z+c)^2}{R_2^9}\right) \tag{34}$$

$$\tau_{23}^{(3)} = \frac{-3F_0 y}{8\pi(1-\sigma)}\left[\frac{1}{R_1^5}-\frac{1}{R_2^5}+\frac{5(z+c)^2}{R_2^7}-\frac{5(z-c)^2}{R_1^7}+\frac{30z(z+c)}{R_2^7}-\frac{70z(z+c)^3}{R_2^9}\right] \tag{35}$$

$$\tau_{31}^{(3)} = \frac{-3F_0 x}{8\pi(1-\sigma)}\left[\frac{1}{R_1^5}-\frac{1}{R_2^5}+\frac{5(z+c)^2}{R_2^7}-\frac{5(z-c)^2}{R_1^7}+\frac{30z(z+c)}{R_2^7}-\frac{70z(z+c)^3}{R_2^9}\right] \tag{36}$$

5 VISCOELASTIC DEFORMATION

The solution for a linear viscoelastic material can be obtained from the elastic one by using the correspondence principle. The bulk modulus κ and the shear modulus μ which are appearing in elastic solution are replaced by $\tilde{\kappa}(s)$ and $\tilde{\mu}(s)$ in viscoelastic solution, which depends on particular rheology considered. The source function $f(t)$ is replaced by its Laplace transform $\tilde{f}(s)$. The resulting expression is the Laplace transformed viscoelastic solution. The solution in the time domain is obtained by inverting it. We assume that the rheology of the viscoelastic half-space is that of a Kelvin, Maxwell and Standard linear solid (SLS).

In the expressions for the displacements and stresses, the elastic moduli κ and μ occur in the following combinations: $J_1 = \frac{1}{2\mu}, Q_1 = \frac{1}{3\kappa+4\mu}, Q_2 = \frac{2\mu}{3\kappa+4\mu}$.

We define $\tilde{J}_1(s) = \frac{1}{2\tilde{\mu}(s)}, \tilde{Q}_1(s) = \frac{1}{3\tilde{\kappa}(s)+4\tilde{\mu}(s)}, \tilde{Q}_2(s) = \frac{2\tilde{\mu}(s)}{3\tilde{\kappa}(s)+4\tilde{\mu}(s)}$, where s is the Laplace transform variable. On inverting, we find that J_1 in the static solution is replaced by $\hat{J}_1(t)$ in the viscoelastic solution, where $\hat{J}_1(t) = L^{-1}\left(\frac{1}{2s\,\tilde{\mu}(s)}\right)$.

Similarly, Q_1 and Q_2 are replaced by the auxiliary functions $\hat{Q}_1(t)$ and $\hat{Q}_2(t)$. For ready reference the values of auxiliary functions [26] for the Kelvin model, Maxwell model, and the SLS model are given below:

For Kelvin model

$\hat{J}_1(t) = J_1\left(1-e^{\frac{-t}{t_1}}\right), \hat{Q}_1(t) = Q_1\left(1-e^{\frac{-At}{t_1}}\right), \hat{Q}_2(t) = Q_2\left(1+\frac{3\kappa}{4\mu}e^{\frac{-At}{t_1}}\right)$, where $A = \frac{3\kappa+4\mu}{4\mu}$, t_1-relaxation time for Kelvin model.

For Maxwell model

$\hat{J}_1(t) = J_1\left(1+\frac{t}{t_2}\right), \hat{Q}_1(t) = Q_1\left(\frac{1}{B}-\frac{4\mu}{3\kappa}e^{\frac{-Bt}{t_2}}\right), \hat{Q}_2(t) = Q_2 e^{\frac{-Bt}{t_2}}$, where $B = \frac{3\kappa}{3\kappa+4\mu}$, t_2-relaxation time for Maxwell model.

For SLS model

$\hat{J}_1(t)=\frac{1}{q_0}\left(1-\left(1-\frac{t_2}{t_1}\right)e^{\frac{-t}{t_1}}\right),\hat{Q}_1(t)=\frac{1}{a_1}\left(1-\frac{2q_0}{b_1}e^{\frac{-t}{t_3}}\right),\hat{Q}_2(t)=\frac{q_0}{a_1}\left(1+\frac{3\kappa}{b_1}e^{\frac{-t}{t_3}}\right)$, where $a_1=3\kappa+2q_0$, $b_1=\frac{3\kappa t_2+2q_0t_1}{t_1-t_2}$, $t_3=\frac{3\kappa t_2+2q_0t_1}{3\kappa+2q_0}$.

SLS model consists of a spring and a Kelvin element in series. If the elastic constants of the two springs are identical, then $q_0=\mu, t_1=2t_2, t_3=\frac{9}{7}t_2$.

6 VISCOELASTIC DISPLACEMENT FIELD

By using elastic displacement field given in section 3, we obtain the viscoelastic displacement field.

6.1 Doublet with an axis parallel to the x-axis

From Eqs. (10)-(12), we obtain the following expressions for the viscoelastic displacement components of Doublet with an axis parallel to the *x*-direction

$$u_1^{(1)}=\frac{F_0}{8\pi}\left[\begin{array}{l}2\hat{J}_1(t)\left(\frac{1}{R_1^3}+\frac{1}{R_2^3}-\frac{6z(z+c)}{R_2^5}-x^2\left(\frac{3}{R_1^5}+\frac{3}{R_2^5}-\frac{30z(z+c)}{R_2^7}\right)\right)\\-3\hat{Q}_1(t)\left(\frac{1}{R_1^3}-\frac{1}{R_2^3}-\frac{6z(z+c)}{R_2^5}-x^2\left(\frac{3}{R_1^5}-\frac{3}{R_2^5}-\frac{30z(z+c)}{R_2^7}\right)\right)\end{array}\right] \tag{37}$$

$$u_2^{(1)}=\frac{-3F_0xy}{8\pi}\left[\left(2\hat{J}_1(t)-3\hat{Q}_1(t)\right)\left(\frac{1}{R_1^5}-\frac{10z(z+c)}{R_2^7}\right)+\frac{\left(2\hat{J}_1(t)+3\hat{Q}_1(t)\right)}{R_2^5}\right] \tag{38}$$

$$u_3^{(1)}=\frac{-3F_0x}{8\pi}\left[\left(2\hat{J}_1(t)-3\hat{Q}_1(t)\right)\left(\frac{z-c}{R_1^5}+\frac{2z}{R_2^5}-\frac{10z(z+c)^2}{R_2^7}\right)-\frac{\left(2\hat{J}_1(t)+3\hat{Q}_1(t)\right)(z+c)}{R_2^5}\right] \tag{39}$$

6.2 Doublet with an axis parallel to the y-axis

From Eqs. (13)-(15), we obtain the following expressions for the viscoelastic displacement components of Doublet with an axis parallel to the *y*-direction

$$u_1^{(2)}=\frac{-3F_0xy}{8\pi}\left[\left(2\hat{J}_1(t)-3\hat{Q}_1(t)\right)\left(\frac{1}{R_1^5}-\frac{10z(z+c)}{R_2^7}\right)+\frac{\left(2\hat{J}_1(t)+3\hat{Q}_1(t)\right)}{R_2^5}\right] \tag{40}$$

$$u_2^{(2)}=\frac{F_0}{8\pi}\left[\begin{array}{l}2\hat{J}_1(t)\left(\frac{1}{R_1^3}+\frac{1}{R_2^3}-\frac{6z(z+c)}{R_2^5}-y^2\left(\frac{3}{R_1^5}+\frac{3}{R_2^5}-\frac{30z(z+c)}{R_2^7}\right)\right)\\-3\hat{Q}_1(t)\left(\frac{1}{R_1^3}-\frac{1}{R_2^3}-\frac{6z(z+c)}{R_2^5}-y^2\left(\frac{3}{R_1^5}-\frac{3}{R_2^5}-\frac{30z(z+c)}{R_2^7}\right)\right)\end{array}\right] \tag{41}$$

$$u_3^{(2)} = \frac{-3F_0\, y}{8\pi}\left[\left(2\hat{J}_1(t)-3\hat{Q}_1(t)\right)\left(\frac{z-c}{{R_1}^5}+\frac{2z}{{R_2}^5}-\frac{10z\,(z+c)^2}{{R_2}^7}\right)-\frac{\left(2\hat{J}_1(t)+3\hat{Q}_1(t)\right)(z+c)}{{R_2}^5}\right] \tag{42}$$

6.3 Doublet with an axis parallel to the z-axis

From Eqs. (16)-(18), we obtain the following expressions for the viscoelastic displacement components of Doublet with an axis parallel to the *z*-direction

$$u_1^{(3)} = \frac{-3F_0 x}{8\pi}\left[\left(2\hat{J}_1(t)-3\hat{Q}_1(t)\right)\left(\frac{z-c}{{R_1}^5}-\frac{2z}{{R_2}^5}+\frac{10z\,(z+c)^2}{{R_2}^7}\right)-\frac{\left(2\hat{J}_1(t)+3\hat{Q}_1(t)\right)(z+c)}{{R_2}^5}\right] \tag{43}$$

$$u_2^{(3)} = \frac{-3F_0 y}{8\pi}\left[\left(2\hat{J}_1(t)-3\hat{Q}_1(t)\right)\left(\frac{z-c}{{R_1}^5}-\frac{2z}{{R_2}^5}+\frac{10z\,(z+c)^2}{{R_2}^7}\right)-\frac{\left(2\hat{J}_1(t)+3\hat{Q}_1(t)\right)(z+c)}{{R_2}^5}\right] \tag{44}$$

$$u_3^{(3)} = \frac{-F_0}{8\pi}\left[\left(2\hat{J}_1(t)-3\hat{Q}_1(t)\right)\left(-\frac{1}{{R_1}^3}+\frac{3(z-c)^2}{{R_1}^5}-\frac{18z\,(z+c)}{{R_2}^5}+\frac{30z\,(z+c)^3}{{R_2}^7}\right)-\left(2\hat{J}_1(t)+3\hat{Q}_1(t)\right)\left(\frac{1}{{R_2}^3}-\frac{3(z+c)^5}{{R_2}^5}\right)\right] \tag{45}$$

7 VISCOELASTIC STRESSES

By using static stress field given in section 4, we obtain the viscoelastic stress field.

7.1 Doublet with an axis parallel to the x-axis

From Eqs. (19)-(24), we obtain the following expressions for the viscoelastic stress components of Doublet with an axis parallel to the *x*-direction

$$\tau_{11}^{(1)} = -\frac{3F_0 x}{4\pi}\left[\begin{array}{l}\left(1-\frac{3}{2}\hat{Q}_2(t)\right)\left(\frac{3}{{R_1}^5}-\frac{3}{{R_2}^5}-\frac{30z\,(z+c)}{{R_2}^7}-5x^2\left(\frac{1}{{R_1}^7}-\frac{14z\,(z+c)}{{R_2}^9}\right)\right)+\left(1+\frac{3}{2}\hat{Q}_2(t)\right)\left(\frac{4}{{R_2}^5}-\frac{5x^2}{{R_2}^7}\right)\\ +\frac{10\left(1-3\hat{Q}_2(t)\right)(z+c)^2}{{R_2}^7}\end{array}\right] \tag{46}$$

$$\tau_{22}^{(1)} = -\frac{3F_0 x}{4\pi}\left[\begin{array}{l}\left(1-\frac{3}{2}\hat{Q}_2(t)\right)\left(\frac{1}{{R_1}^5}-\frac{3}{{R_2}^5}-\frac{10z\,(z+c)}{{R_2}^7}-5y^2\left(\frac{1}{{R_1}^7}-\frac{14z\,(z+c)}{{R_2}^9}\right)\right)\\ +\left(1+\frac{3}{2}\hat{Q}_2(t)\right)\left(\frac{2}{{R_2}^5}-\frac{5y^2}{{R_2}^7}\right)+\frac{10\left(1-3\hat{Q}_2(t)\right)(z+c)^2}{{R_2}^7}\end{array}\right] \tag{47}$$

$$\tau_{33}^{(1)} = -\frac{3F_0\, x\left(1-\frac{3}{2}\hat{Q}_2(t)\right)}{4\pi}\left[\frac{1}{{R_1}^5}-\frac{1}{{R_2}^5}-\frac{5(z-c)^2}{{R_1}^7}-\frac{5(z+c)(5z-c)}{{R_2}^7}+\frac{10z\,(z+c)^3}{{R_2}^9}\right] \tag{48}$$

$$\tau_{12}^{(1)}=\frac{-3F_0\,y}{4\pi}\left[\left(1-\frac{3}{2}\hat{Q}_2(t)\right)\left(\frac{1}{{R_1}^5}-\frac{10z\,(z+c)}{{R_2}^7}-5x^2\left(\frac{1}{{R_1}^7}-\frac{14z\,(z+c)}{{R_2}^9}\right)\right)+\left(1+\frac{3}{2}\hat{Q}_2(t)\right)\left(\frac{1}{{R_2}^5}-\frac{5x^2}{{R_2}^7}\right)\right] \tag{49}$$

$$\tau_{23}^{(1)}=\frac{-15F_0\,x\,y}{4\pi}\left[\left(1-\frac{3}{2}\hat{Q}_2(t)\right)\left(-\frac{z-c}{{R_1}^7}-\frac{(3z+c)}{{R_2}^7}+\frac{14z\,(z+c)^2}{{R_2}^9}\right)\right] \tag{50}$$

$$\tau_{31}^{(1)}=\frac{-3F_0}{4\pi}\left(1-\frac{3}{2}\hat{Q}_2(t)\right)\left[\frac{z-c}{{R_1}^5}+\frac{(3z+c)}{{R_2}^5}-\frac{10z\,(z+c)^2}{{R_2}^7}-5x^2\left(\frac{z-c}{{R_1}^7}+\frac{(3z+c)}{{R_2}^7}-\frac{14z\,(z+c)^2}{{R_2}^9}\right)\right] \tag{51}$$

7.2 Doublet with an axis parallel to the y-axis

From Eqs. (25)-(30), we obtain the following expressions for the viscoelastic stress components of Doublet with an axis parallel to the *y*-direction

$$\tau_{11}^{(2)}=-\frac{3F_0\,y}{4\pi}\left[\begin{array}{l}\left(1-\frac{3}{2}\hat{Q}_2(t)\right)\left(\frac{1}{{R_1}^5}-\frac{3}{{R_2}^5}-\frac{10z\,(z+c)}{{R_2}^7}-5x^2\left(\frac{1}{{R_1}^7}-\frac{14z\,(z+c)}{{R_2}^9}\right)\right)\\+\left(1+\frac{3}{2}\hat{Q}_2(t)\right)\left(\frac{2}{{R_2}^5}-\frac{5x^2}{{R_2}^7}\right)+\frac{10\left(1-3\hat{Q}_2(t)\right)(z+c)^2}{{R_2}^7}\end{array}\right] \tag{52}$$

$$\tau_{22}^{(2)}=-\frac{3F_0\,y}{4\pi}\left[\begin{array}{l}\left(1-\frac{3}{2}\hat{Q}_2(t)\right)\left(\frac{3}{{R_1}^5}-\frac{3}{{R_2}^5}-\frac{30z\,(z+c)}{{R_2}^7}-5y^2\left(\frac{1}{{R_1}^7}-\frac{14z\,(z+c)}{{R_2}^9}\right)\right)\\+\left(1+\frac{3}{2}\hat{Q}_2(t)\right)\left(\frac{4}{{R_2}^5}-\frac{5y^2}{{R_2}^7}\right)+\frac{10\left(1-3\hat{Q}_2(t)\right)(z+c)^2}{{R_2}^7}\end{array}\right] \tag{53}$$

$$\tau_{33}^{(2)}=-\frac{3F_0\,y\left(1-\frac{3}{2}\hat{Q}_2(t)\right)}{4\pi}\left[\frac{1}{{R_1}^5}-\frac{1}{{R_2}^5}-\frac{5(z+c)(5z-c)}{{R_2}^7}-\frac{5(z-c)^2}{{R_1}^7}+\frac{10z\,(z+c)^3}{{R_2}^9}\right] \tag{54}$$

$$\tau_{12}^{(2)}=\frac{-3F_0\,x}{4\pi}\left[\left(1-\frac{3}{2}\hat{Q}_2(t)\right)\left(\frac{1}{{R_1}^5}-\frac{10z\,(z+c)}{{R_2}^7}-5y^2\left(\frac{1}{{R_1}^7}-\frac{14z\,(z+c)}{{R_2}^9}\right)\right)+\left(1+\frac{3}{2}\hat{Q}_2(t)\right)\left(\frac{1}{{R_2}^5}-\frac{5y^2}{{R_2}^7}\right)\right] \tag{55}$$

$$\tau_{23}^{(2)}=\frac{-3F_0\left(1-\frac{3}{2}\hat{Q}_2(t)\right)}{4\pi}\left[\frac{z-c}{{R_1}^5}+\frac{(3z+c)}{{R_2}^5}-\frac{10z\,(z+c)^2}{{R_2}^7}-5y^2\left(\frac{z-c}{{R_1}^7}+\frac{(3z+c)}{{R_2}^7}-\frac{14z\,(z+c)^2}{{R_2}^9}\right)\right] \tag{56}$$

$$\tau_{31}^{(2)}=\frac{-15F_0\,x\,y\,\left(1-\frac{3}{2}\hat{Q}_2(t)\right)}{4\pi}\left(-\frac{z-c}{{R_1}^7}-\frac{(3z+c)}{{R_2}^7}+\frac{14z\,(z+c)^2}{{R_2}^9}\right) \tag{57}$$

7.3 Doublet with an axis parallel to the z-axis

From Eqs. (31)-(36), we obtain the following expressions for the viscoelastic stress components of Doublet with an axis parallel to the *z*-direction

$$\tau_{11}^{(3)}=-\frac{3F_0}{4\pi}\left[\begin{array}{l}\left(1-\frac{3}{2}\hat{Q}_2(t)\right)\left(\frac{z-c}{R_1^5}-\frac{2z}{R_2^5}+\frac{9(z+c)}{R_2^5}+\frac{10z(z+c)^2}{R_2^7}-5x^2\left(\frac{z-c}{R_1^7}-\frac{2z}{R_2^7}+\frac{14z(z+c)^2}{R_2^9}\right)\right)\\+\left(1+\frac{3}{2}\hat{Q}_2(t)\right)\left(-\frac{4(z+c)}{R_2^5}+\frac{5x^2(z+c)}{R_2^7}\right)-\frac{10\left(1-3\hat{Q}_2(t)\right)(z+c)^3}{R_2^7}\end{array}\right] \tag{58}$$

$$\tau_{22}^{(3)}=-\frac{3F_0}{4\pi}\left[\begin{array}{l}\left(1-\frac{3}{2}\hat{Q}_2(t)\right)\left(\frac{z-c}{R_1^5}-\frac{2z}{R_2^5}+\frac{9(z+c)}{R_2^5}+\frac{10z(z+c)^2}{R_2^7}-5y^2\left(\frac{z-c}{R_1^7}-\frac{2z}{R_2^7}+\frac{14z(z+c)^2}{R_2^9}\right)\right)\\+\left(1+\frac{3}{2}\hat{Q}_2(t)\right)\left(-\frac{4(z+c)}{R_2^5}+\frac{5y^2(z+c)}{R_2^7}\right)-\frac{10\left(1-3\hat{Q}_2(t)\right)(z+c)^3}{R_2^7}\end{array}\right] \tag{59}$$

$$\tau_{33}^{(3)}=-\frac{3F_0\left(1-\frac{3}{2}\hat{Q}_2(t)\right)}{4\pi}\left[\frac{3(z-c)}{R_1^5}+\frac{3(z+c)}{R_2^5}-\frac{6z}{R_2^5}-\frac{5(z+c)^3}{R_2^7}-\frac{5(z-c)^3}{R_1^7}+\frac{60z(z+c)^2}{R_2^7}-\frac{70z(z+c)^4}{R_2^9}\right] \tag{60}$$

$$\tau_{12}^{(3)}=\frac{-15F_0xy}{4\pi}\left[\left(1-\frac{3}{2}\hat{Q}_2(t)\right)\left(-\frac{z-c}{R_1^7}+\frac{2z}{R_2^7}-\frac{14z(z+c)^2}{R_2^9}\right)+\left(1+\frac{3}{2}\hat{Q}_2(t)\right)\frac{(z+c)}{R_2^7}\right] \tag{61}$$

$$\tau_{23}^{(3)}=-\frac{3F_0y\left(1-\frac{3}{2}\hat{Q}_2(t)\right)}{4\pi}\left[\frac{1}{R_1^5}-\frac{1}{R_2^5}+\frac{5(z+c)^2}{R_2^7}-\frac{5(z-c)^2}{R_1^7}+\frac{30z(z+c)}{R_2^7}-\frac{70z(z+c)^3}{R_2^9}\right] \tag{62}$$

$$\tau_{31}^{(3)}=-\frac{3F_0x\left(1-\frac{3}{2}\hat{Q}_2(t)\right)}{4\pi}\left[\frac{1}{R_1^5}-\frac{1}{R_2^5}+\frac{5(z+c)^2}{R_2^7}-\frac{5(z-c)^2}{R_1^7}+\frac{30z(z+c)}{R_2^7}-\frac{70z(z+c)^3}{R_2^9}\right] \tag{63}$$

8 NUMERICAL RESULTS AND DISCUSSION

We define dimensionless epicentral distance *D*, dimensionless horizontal displacements U_1, U_2 (with axis parallel to *x*-axis), dimensionless uplifts W_1, W_2 (with axis parallel to *z*-axis), dimensionless stresses Γ_{x1},Γ_{y1} (with axis parallel to *x*-axis) and Γ_{x2},Γ_{y2} (with axis parallel to *z*-axis) by the relations:

$$D=\frac{x}{c},U_1=\frac{A}{c}u_1^{(1)},W_1=\frac{A}{c}u_1^{(3)},U_2=\frac{A}{c}u_3^{(1)},W_2=\frac{A}{c}u_3^{(3)},\Gamma_{x1}=\frac{A}{\mu}\tau_{11}^{(1)},\Gamma_{y1}=\frac{A}{\mu}\tau_{22}^{(1)},$$

$$\Gamma_{x2}=\frac{A}{\mu}\tau_{11}^{(3)}\text{ and }\Gamma_{y2}=\frac{A}{\mu}\tau_{22}^{(3)}$$

where $A=\frac{4\pi\mu c^4}{F_0}$ is dimensionless constant.

For further calculations, the following assumptions are taken place: half-space $z \geq 0$ is stress free at z =0, the bulk modulus κ and the shear modulus μ of viscoelastic half-space satisfy Poisson's condition $\frac{\kappa}{\mu} = \frac{5}{3}$. We also assumed that t > 0 and the source time function is the Heaviside step function. We are using the values of various auxiliary functions as given above in viscoelastic deformation when the material is elastic in dilatation and Kelvin, Maxwell or an SLS type viscoelastic in distortion.

8.1 Elastic displacements

By using above conditions and Eqs. (10) - (18), we find dimensionless elastic displacements.

8.1.1 Elastic displacements with axis parallel to x-axis

$$U_1 = \frac{1-2D^2}{\left(D^2+1\right)^{\frac{5}{2}}} \tag{64}$$

$$U_2 = \frac{3D}{\left(D^2+1\right)^{\frac{5}{2}}} \tag{65}$$

8.1.2 Elastic displacements with axis parallel to z-axis

$$W_1 = \frac{3D}{\left(D^2+1\right)^{\frac{5}{2}}} \tag{66}$$

$$W_2 = \frac{D^2-2}{\left(D^2+1\right)^{\frac{5}{2}}} \tag{67}$$

8.2 Viscoelastic displacements

By using above conditions and Eqs. (37) - (45), we find dimensionless viscoelastic displacements

8.2.1 Viscoelastic displacements for Kelvin model with axis parallel to x-axis

$$U_1 = \frac{\left(1-2D^2\right)\left(1-e^{-T}\right)}{\left(D^2+1\right)^{\frac{5}{2}}} \tag{68}$$

$$U_2 = \frac{3D\left(1-e^{-T}\right)}{\left(D^2+1\right)^{\frac{5}{2}}} \tag{69}$$

8.2.2 Viscoelastic displacements for Kelvin model with axis parallel to z-axis

$$W_1 = \frac{3D\left(1-e^{-T}\right)}{\left(D^2+1\right)^{\frac{5}{2}}} \tag{70}$$

$$W_2 = \frac{\left(D^2-2\right)\left(1-e^{-T}\right)}{\left(D^2+1\right)^{\frac{5}{2}}} \tag{71}$$

where $T = \frac{t}{t_1}$, t_1-relaxation time for Kelvin model.

8.2.3 Viscoelastic displacements for Maxwell model with axis parallel to x-axis

$$U_1 = \frac{\left(1-2D^2\right)(1+T)}{\left(D^2+1\right)^{\frac{5}{2}}} \tag{72}$$

$$U_2 = \frac{3D\left(1+T\right)}{\left(D^2+1\right)^{\frac{5}{2}}} \tag{73}$$

8.2.4 Viscoelastic displacements for Maxwell model with axis parallel to z-axis

$$W_1 = \frac{3D\left(1+T\right)}{\left(D^2+1\right)^{\frac{5}{2}}} \tag{74}$$

$$W_2 = \frac{\left(D^2-2\right)(1+T)}{\left(D^2+1\right)^{\frac{5}{2}}} \tag{75}$$

where $T = \frac{t}{t_2}$, t_2-relaxation time for Maxwell model.

8.2.5 Viscoelastic displacements for SLS model with axis parallel to x-axis

$$U_1 = \frac{\left(1-2D^2\right)\left(1-\frac{1}{2}e^{\frac{-1}{2}T}\right)}{\left(D^2+1\right)^{\frac{5}{2}}} \tag{76}$$

$$U_2 = \frac{3D\left(1-\frac{1}{2}e^{\frac{-1}{2}T}\right)}{\left(D^2+1\right)^{\frac{5}{2}}} \tag{77}$$

8.2.6 Viscoelastic displacements for SLS model with axis parallel to z-axis

$$W_1 = \frac{3D\left(1-\frac{1}{2}e^{\frac{-1}{2}T}\right)}{\left(D^2+1\right)^{\frac{5}{2}}} \tag{78}$$

$$W_2 = \frac{\left(D^2-2\right)\left(1-\frac{1}{2}e^{\frac{-1}{2}T}\right)}{\left(D^2+1\right)^{\frac{5}{2}}} \tag{79}$$

where $T = \frac{t}{t_2}$, t_2 -relaxation time for SLS model.

8.3 Elastic stresses

By using above conditions and equations from (19)-(36) we get dimensionless elastic stresses

8.3.1 Elastic stresses with axis parallel to x-axis

$$\Gamma_{x1} = \frac{-6D}{\left(D^2+1\right)^{\frac{5}{2}}}\left[\frac{3-4\sigma}{1-\sigma}+\frac{5\sigma}{(1-\sigma)\left(D^2+1\right)}-\frac{5D^2}{\left(D^2+1\right)}\right] \tag{80}$$

$$\Gamma_{y1} = \frac{-6D}{(1-\sigma)\left(D^2+1\right)^{\frac{5}{2}}}\left[(1-2\sigma)+\frac{5\sigma}{\left(D^2+1\right)}\right] \tag{81}$$

8.3.2 Elastic stresses with axis parallel to z-axis

$$\Gamma_{x2} = \frac{6}{\left(D^2+1\right)^{\frac{5}{2}}}\left[\frac{1-4\sigma}{1-\sigma}+\frac{5\sigma}{(1-\sigma)\left(D^2+1\right)}-\frac{5D^2}{\left(D^2+1\right)}\right] \tag{82}$$

$$\Gamma_{y2} = \frac{6}{(1-\sigma)\left(D^2+1\right)^{\frac{5}{2}}}\left[(1-4\sigma)+\frac{5\sigma}{\left(D^2+1\right)}\right] \tag{83}$$

8.4 Viscoelastic stresses

By using above conditions and Eqs. (46) - (63), we find dimensionless viscoelastic stresses.

8.4.1 Viscoelastic stresses with axis parallel to x-axis

$$\Gamma_{x1} = \frac{-6D}{\left(D^2+1\right)^{\frac{7}{2}}}\left[7-3D^2+3\hat{Q}_2(t)\left(D^2-4\right)\right] \tag{84}$$

$$\Gamma_{y1} = \frac{-6D}{\left(D^2+1\right)^{\frac{7}{2}}}\left[5+3\hat{Q}_2(t)\left(D^2-4\right)\right] \tag{85}$$

8.4.2 Viscoelastic stresses with axis parallel to z-axis

$$\Gamma_{x2} = \frac{-6}{\left(D^2+1\right)^{\frac{7}{2}}}\left[7D^2-3-3\hat{Q}_2(t)\left(3D^2+7\right)\right] \tag{86}$$

$$\Gamma_{y2} = \frac{-6}{\left(D^2+1\right)^{\frac{7}{2}}}\left[2D^2-3-3\hat{Q}_2(t)\left(3D^2-2\right)\right] \tag{87}$$

where for Kelvin model $\hat{Q}_2(t) = \frac{2}{9}\left(1+\frac{5}{4}e^{\frac{-9}{4}T}\right)$ and $T = \frac{t}{t_1}$, t_1-relaxation time for Kelvin model.

For Maxwell model

$\hat{Q}_2(t) = \frac{2}{9}e^{\frac{-5}{9}T}$ and $T = \frac{t}{t_2}$, t_2-relaxation time for Maxwell model.

For SLS model

$\hat{Q}_2(t) = \frac{1}{7}\left(1+\frac{5}{9}e^{\frac{-7}{9}T}\right)$ and $T = \frac{t}{t_2}$, t_2-relaxation time for SLS model.

Fig. 4 shows the variation of the dimensionless horizontal displacement U_1 with the dimensionless epicentral distance. We note that it assumes maximum value $U_1 = 1$ at D = 0 after that it decreases with D and attains minimum value $U_1 = -0.2$ at $D = 1$. Further increase slightly with D and become constant as D tends to infinity.

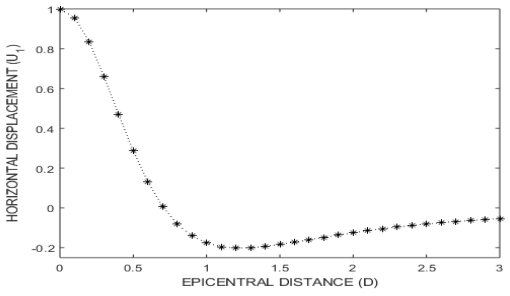

Fig.4
Variation of the dimensionless horizontal displacement (U_1) with the dimensionless epicentral distance (D).

Fig. 5 shows the variation of the dimensionless horizontal displacement (U_2) with the dimensionless epicentral distance. We note that it increases with epicentral distance and attains maximum value between D=0.5 to D=1 after that it decreases rapidly and tends to zero as epicentral distance increases.

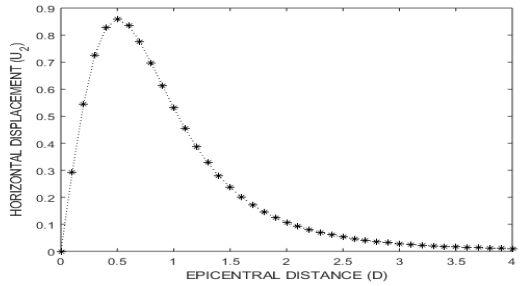

Fig.5
Variation of the dimensionless horizontal displacement (U_2) with the dimensionless epicentral distance (D).

Fig. 6 shows the variation of the dimensionless uplift (W_1) with the dimensionless epicentral distance. We note that Figs. 5 and 6 both have the same pattern.

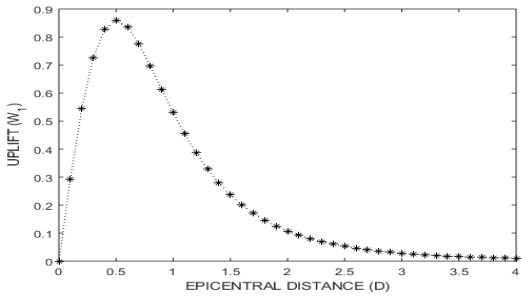

Fig.6
Variation of the dimensionless uplift (W_1) with the dimensionless epicentral distance (D).

Fig.7 shows the variation of the dimensionless uplift (W_2) with the dimensionless epicentral distance. It increases with D and tends to zero at D=1.5 onwards.

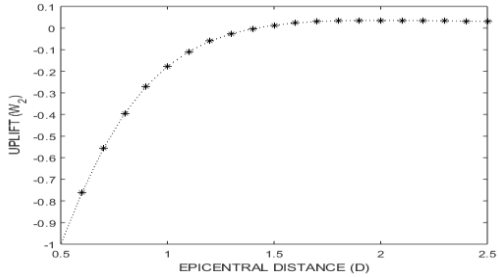

Fig.7
Variation of the dimensionless uplift (W_2) with the dimensionless epicentral distance (D).

Fig. 8 shows the variation of the dimensionless stress Γ_{x1} with the dimensionless epicentral distance for various values of σ. We note that it first decreases and then increases with D = 0 to 1 and beyond that limit, it tends to zero. It attains minimum value -9.5 at D = 0.4 for Poissonian half space.

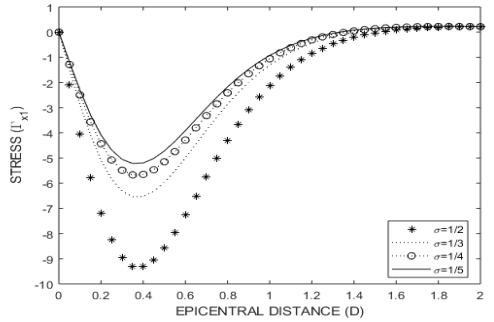

Fig.8
Variation of the dimensionless stress Γ_{x1} with the dimensionless epicentral distance for various values of σ.

Fig. 9 shows the variation of the dimensionless stress Γ_{y1} with the dimensionless epicentral distance for various values of σ . We note that it attains minimum value -7.5 at *D* =0.4 for Poissonian half space.

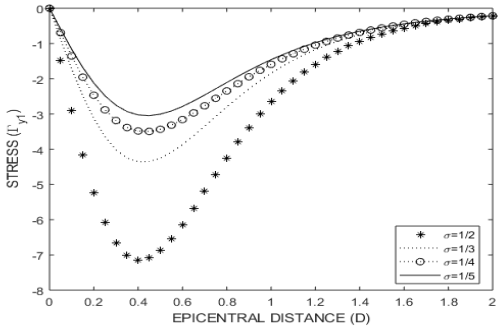

Fig.9
Variation of the dimensionless stress Γ_{y1} with the dimensionless epicentral distance for various values of σ .

Fig.10 shows the variation of the dimensionless stress Γ_{x2} with the dimensionless epicentral distance for various values of σ . We note that it attains maximum value $\Gamma_{x2} = 18$ and minimum value -2.3 at $\sigma = 1/2$. For large values of *D*, the curves tend to merge.

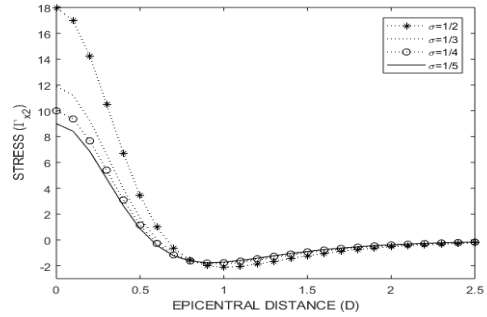

Fig.10
Variation of the dimensionless stress Γ_{x2} with the dimensionless epicentral distance for various values of σ .

Fig. 11 shows the variation of the dimensionless stress Γ_{y2} with the dimensionless epicentral distance for various values of σ . We note that it attains maximum value $\Gamma_{y2} = 0.9$ and minimum -0.17. For large values of *D*, the curves going to merge and tends to zero.

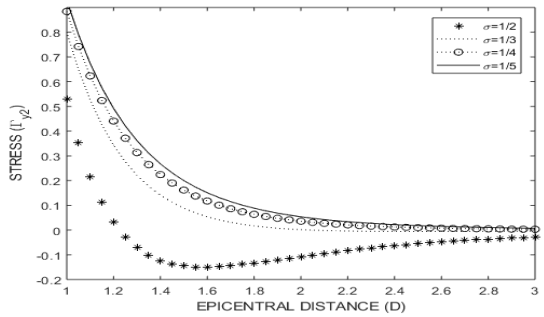

Fig.11
Variation of the dimensionless stress Γ_{y2} with the dimensionless epicentral distance for various values of σ .

Fig. 12 shows the variation of horizontal displacements U_1 and U_2 for the three models, namely Kelvin, a Maxwell and a SLS with the epicentral distance for different values of *T*. We note that in case of all the three models horizontal displacement U_1 goes on decreasing with epicentral distance and decrease of *T*. They merge at some point and approaches to zero as shown in Fig. 12(a). U_2 increases and then decreases with *D* as shown in Fig. 12(b). The elastic displacement coincides with the viscoelastic displacement at *T*=0.

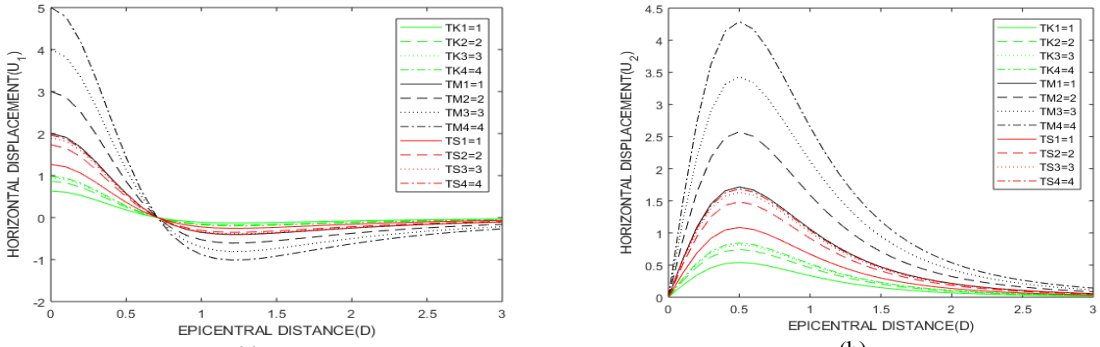

(a) (b)

Fig.12
Variation of the dimensionless horizontal displacements (U_1 and U_2) with the dimensionless epicentral distance for the various values of T for Kelvin, Maxwell, and SLS model.

The extremum values of the horizontal displacements U_1 and U_2 are given in Table 1. Horizontal displacements attain the maximum value in case of Maxwell and minimum in case of Kelvin for a particular value of time.

Table 1
Extremum values of horizontal displacements with axis parallel to x-axis.

Horizontal displacements	Extremum values of horizontal displacements U_1 and U_2		
	Kelvin	Maxwell	SLS
U_1	0.99	5	1.8
U_2	0.8	4.3	1.6

Fig. 13 shows the variation of uplift W_1 and W_2 for the three models, namely Kelvin, a Maxwell and an SLS with the epicentral distance for different values of T. We note that in case of all the three models uplift W_1 is same as horizontal displacement U_2 as shown in Fig. 13(a). Uplift W_2 is negative and increases with D and T as shown in Fig. 13(b). They merge at some point and approaches to zero. The elastic displacement coincides with the viscoelastic displacement at T=0.

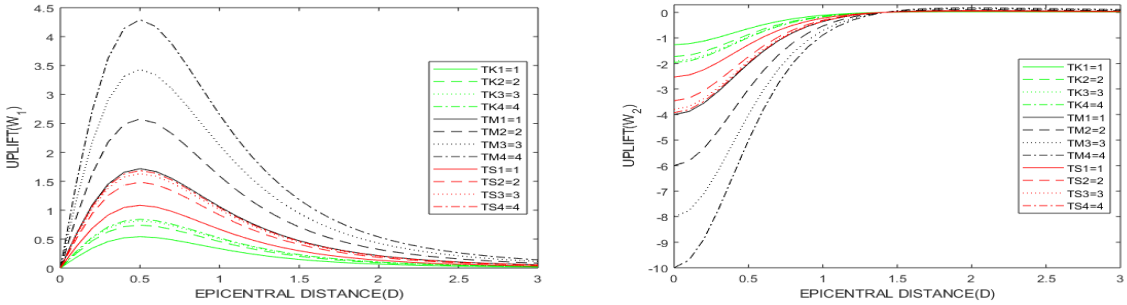

(a) (b)

Fig.13
Variation of the dimensionless uplift (W_1 and W_2) with the dimensionless epicentral distance for the various values of T for Kelvin, Maxwell, and SLS model.

The extremum values of uplift W_1 (same as U_2) and W_2 are given in Table 2. Numerically both Uplifts W_1 and W_2 assumes the maximum value in case of Maxwell and minimum in case of Kelvin model for a particular value of time.

Table 2
Extremum values of Uplift with axis parallel to *z*-axis.

Uplift	Extremum values of Uplift W_1 and W_2		
	Kelvin	Maxwell	SLS
W_1	0.8	4.3	1.6
W_2	-1.99	-10	-3.9

Fig. 14 shows the variation of the dimensionless stress Γ_{x1} and Γ_{y1} along the x-axis for the three models, namely Kelvin, a Maxwell and an SLS with the epicentral distance for various values of *T*. We note that stresses are negative for all epicentral distances and it decreases first and then increases and then approaches to zero with *D* as shown in Fig. 14.

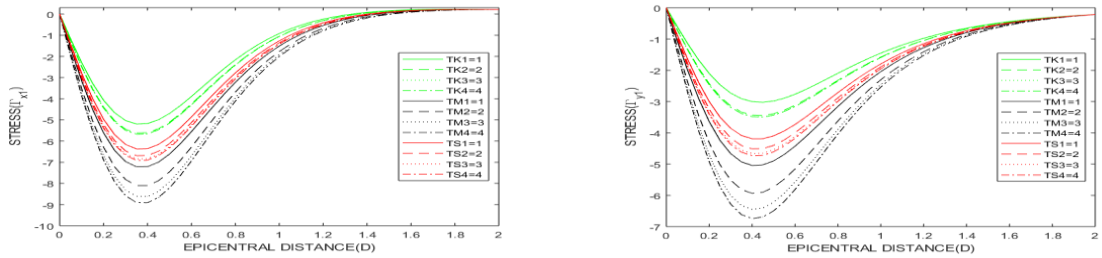

(a) (b)

Fig.14
Variation of the dimensionless stress Γ_{x1} and Γ_{y1} with the dimensionless epicentral distance along the *x*-axis for the various values of *T* for Kelvin, Maxwell, and SLS model.

The extremum values of the dimensionless stress Γ_{x1} and Γ_{y1} with axis parallel to *x*-axis are given in Table 3. Numerically Maxwell gives maximum values for stresses and Kelvin gives minima.

Table 3
Extremum values of Stresses with axis parallel to x-axis

Stresses	Extremum values of Stresses Γ_{x1} and Γ_{y1}		
	Kelvin	Maxwell	SLS
Γ_{x1}	-5.99	-9	-7
Γ_{y1}	-3.5	-6.9	-4.9

Fig. 15 shows the variation of the dimensionless stresses Γ_{x2} and Γ_{y2} along the *z*-axis for the three models, namely Kelvin, a Maxwell and SLS with the epicentral distance for various values of *T*. We note that stresses are positive for all epicentral distances and it decreases and approaches to zero with *D* as shown in Fig. 15.

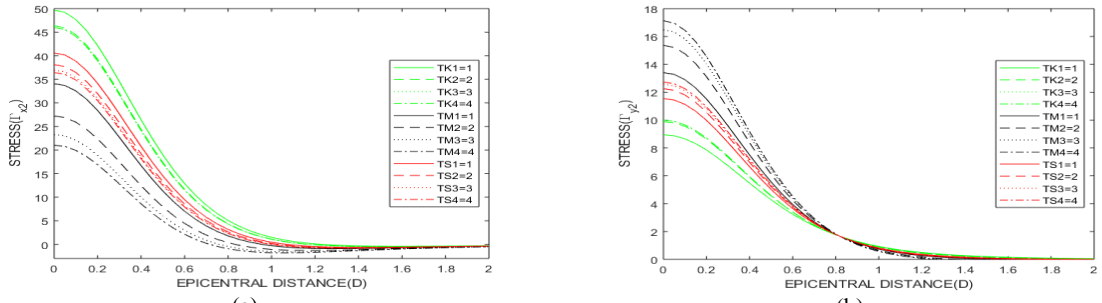

(a) (b)

Fig.15
Variation of the dimensionless stress Γ_{x2} and Γ_{y2} with the dimensionless epicentral distance along the *z*-axis for the various values of *T* for Kelvin, Maxwell, and SLS model.

The extremum values of the dimensionless stresses Γ_{x2} and Γ_{y2} with axis parallel to *z*-axis are given in Table 4. Γ_{x2} attains the maximum value in case of Kelvin and minimum in case of Maxwell and Γ_{y2} assume the maximum value in case of Maxwell and minimum in case of Kelvin for a particular value of time.

Table 4
Extremum values of Stresses with axis parallel to *z*-axis.

Stresses	Extremum values of Stresses Γ_{x2} and Γ_{y2}		
	Kelvin	Maxwell	SLS
Γ_{x2}	50	34.8	40.05
Γ_{y2}	10	17.2	12.8

9 CONCLUSION

The explicit expressions for the displacement and stress fields in an elastic and viscoelastic half-space due to a doublet source have been obtained by using Galerkin vector approach. The results are valid for arbitrary values of Poisson's ratio. The effect of relaxation time on the deformation field has been examined. The variation of the displacement and stresses with the epicentral distance have been studied graphically. The horizontal displacement U_2 shows the same effects as uplift W_1 with the epicentral distance. In case of all the three models Kelvin, Maxwell, SLS models uplift W_1 has the same effect as horizontal displacement U_2. Stresses for doublet with axis parallel to *x*-axis attain minimum value for Poissonian half space. Viscoelastic displacements and stresses attain maxima for Maxwell model and minima for Kelvin model. The displacement field obtained for a doublet source is coinciding with the results of Okada [7] by starting with the results of concentrated point source by superposition & differentiation.

ACKNOWLEDGMENTS

One of the author Ms. Nishu Verma is grateful to the University Grants Commission, New Delhi for financial support.

REFERENCES

[1] Singh S.J., Ben-Menahem A., 1969, Displacement and strain fields due to faulting in a sphere, *Physics of the Earth and Planetary Interiors* **2**: 77-87.
[2] Singh S.J., 1970, Static deformation of a multilayered half-space by internal sources, *Journal of Geophysical Research* **75**: 3257-3263.
[3] Singh S.J., Ben-Menahem A., Vered M., 1973, A unified approach to the representation of seismic sources, *Proceedings of The Royal Society of London A* **331**: 525-551.
[4] Freund L.B., Barnett D.M., 1976, A two-dimensional analysis of surface deformation due to dip-slip faulting, *Bulletin of the Seismological Society of America* **66**: 667-675.
[5] Aki K., Richards P.G., 1980, *Quantitative Seismology: Theory and Methods*, San Francisco.
[6] Stein S., Wysession M., 2003, *An Introduction to Seismology, Earthquakes, and Earth Structure*, Blackwell Publishing, Oxford.
[7] Okada Y., 1985, Surface deformation due to shear and tensile faults in a half-space, *Bulletin of the Seismological Society of America* **75**: 1135-1154.
[8] Bonafede M., Dragoni M., Quareni F., 1986, Displacement and stress fields produced by a center of dilatation and by a pressure source in a viscoelastic half-space: application to the study of ground deformation and seismic activity at vampi flegeri, *Geophysical Journal International* **87**: 455-485.
[9] Singh K., Singh S.J., 1989, Static and quasi-static deformation of a uniform half space by buried sources, *Geophysical Journal International* **27**: 1-30.
[10] Roberts P.M., Phillips W.S., Fehler, M.C., 1992, Development of the active doublet method for measuring small velocity and attenuation changes in solids, *Journal of the Acoustical Society of America* **91**: 3291.

[11] Horikawa H., 2001, Earthquake doublet in kagoshima, Japan: rupture of asperities in a stress shadow, *Bulletin of the Seismological Society of America* **91**:112-127.
[12] Pandolfi D., Bean C.J., Saccorotti G., 2006, Coda wave interferometric detection of seismic velocity changes associated with the 1999 $M = 3.6$ event at Mt. vesuvius, *Geophysical Research Letters* **33**: L06306.
[13] Wang R., Lorenzo-Martin F., Roth F., 2006, PSGRN/PSCMP- a new code for calculating co- and post-seismic deformation, geoid and gravity changes based on the viscoelastic-gravitational dislocation theory, *Computer & Geosciences* **32**: 527-541.
[14] Lin C.H., Yeh Y.H., Ando M., 2008, Earthquake doublet sequences: evidence of static triggering in the strong convergent zones of taiwan, *Terrestrial Atmospheric and Oceanic Sciences* **19**: 589-594.
[15] Lai K.Y., Chen Y.G., Wu Y.M., 2009, The 2005 Ilan earthquake doublet and seismic crisis in northeastern Taiwan: evidence for dyke intrusion associated with on-land propagation of the Okinawa Trough, *Geophysical Journal International* **179**: 678-686.
[16] Kogan M.G., Vasilenko N.F., Frolov D.I., 2011, The mechanism of postseismic deformation triggered by the 2006-2007 great kurli earthquakes, *Geophysical Research Letters* **38**: L06304.
[17] Donnera S., Ghodsb A., Krugera F., 2015, The Ahar-Varzeghan earthquake doublet ($\boldsymbol{M}_w$ 6.4 and 6.2) on 11 August 2012: Regional Seismic Moment Tensors and a Seismotectonic Interpretation, *Bulletin of the Seismological Society of America* **105**: 791-807.
[18] Nissen E., Elliott J.R., Solan R.A., 2016, Limitations of rupture forecasting exposed by instantaneously triggered earthquake doublet, *Nature Geoscience* **9**(4): 330-336.
[19] Verma N., and Singh K., 2020a, Deformation of two welded half-spaces caused by a centre of rotation source, *Physics of the Earth and Planetary Interiors* **299**(106410): 1-12.
[20] Verma N., Singh K., 2020b, A comparative study of deformation field due to center of dilatation and center of rotation in a viscoelastic half-space model, *Physics of the Earth and Planetary Interiors* **299**(106428), 1-7.
[21] Granik V.T., Ferrari M., 1993, Microstructural mechanics of granular media, *Mechanics of Materials* **15**: 301-322.
[22] Ferrari M., Granik V.T., Imam A., Nadeau J., 1997, *Advance in Doublet Mechanics*, Springer.
[23] Sadd M.H., Dai Q.L., Parameswaran V., Shukla A., 2004a, Microstructural simulation of asphalt materials: modelling and experimental studies, *Journal of Civil Engineering* **16**(2): 107-115.
[24] Mindlin R.D., Cheng D.H., 1950, Nuclei of strain in the semi-infinite solid, *Journal of Applied Physics* **21**: 926-930.
[25] Mindlin R.D., 1936, Force at a point in the interior of a semi-infinite solid, *Journal of Applied Physics* **7**: 195-202.
[26] Singh K., Singh S.J., 1990, Simple procedure for obtaining the quasi-static displacement, strains, and stresses in a viscoelastic half-space, *Bulletin of the Seismological Society of America* **80**: 488-492.